Journal of Nuclear Materials 392 (2009) 139–150

Contents lists available at ScienceDirect

Journal of Nuclear Materials

journal homepage: www.elsevier.com/locate/jnucmat

Metallic fuels for advanced reactors

W.J. Carmack [a,*], D.L. Porter [a], Y.I. Chang [b], S.L. Hayes [a], M.K. Meyer [a], D.E. Burkes [a], C.B. Lee [c], T. Mizuno [d], F. Delage [e], J. Somers [f]

[a] Nuclear Fuels and Materials Division, Idaho National Laboratory, Idaho Falls, ID 83415-6188, USA
[b] Argonne National Laboratory, 9700 S. Cass Avenue, Argonne, IL 60439, USA
[c] Korea Atomic Energy Research Institute, 1045 Daedeok-daero, Yuseong, Daejeon 305-353, Republic of Korea
[d] Japan Atomic Energy Agency, 4002 Narita-cho, O-arai-machi, O-arai R&D Center, Japan
[e] Commission of Energie Atomic, CE A/Cadarache – Batiment 717, 13108 Saint-Paul-Iez-Durance Cedex, France
[f] Institute of Transuranium Elements, Directorate General JRC, P.O. Box 2340, Karlsruhe 76125, Germany

A B S T R A C T

In the framework of the Generation IV Sodium Fast Reactor Program, the Advanced Fuel Project has conducted an evaluation of the available fuel systems supporting future sodium cooled fast reactors. This paper presents an evaluation of metallic alloy fuels. Early US fast reactor developers originally favored metal alloy fuel due to its high fissile density and compatibility with sodium. The goal of fast reactor fuel development programs is to develop and qualify a nuclear fuel system that performs all of the functions of a conventional fast spectrum nuclear fuel while destroying recycled actinides. This will provide a mechanism for closure of the nuclear fuel cycle. Metal fuels are candidates for this application, based on documented performance of metallic fast reactor fuels and the early results of tests currently being conducted in US and international transmutation fuel development programs.

1. Introduction

Fast reactor development programs have been conducted over the past five decades. Early US fast reactor developers originally favored metal alloy fuel due to its high fissile density and compatibility with sodium. As metal alloy fuels continued to be developed it was discovered that low smear density allowed the fuel to operate to much higher burnup. The goal of fuel development programs for future fast reactors is to develop and qualify for operation, a nuclear fuel system that performs all of the functions of a conventional fast spectrum nuclear fuel while destroying recycled actinides. This fuel would provide a mechanism for closure of the nuclear fuel cycle. Metal fuels are candidates for this application, based on documented performance of metallic fast reactor fuels and the early results of fuel tests currently being conducted in U.S. and international transmutation fuel development programs.

Metal fuel shown schematically in Fig. 1 was selected for fueling many of the first reactors in the US, including the Experimental Breeder Reactor-I (EBR-I) and the Experimental Breeder Reactor-II (EBR-II) in Idaho, the FERMI-I reactor, and the Dounreay Fast Reactor (DFR) in the UK [1,2]. Metallic U–Pu–Zr alloys were the reference fuel for the US Integral Fast Reactor (IFR) program. An extensive database on the performance of advanced metal fuels was generated as a result of the operation of these reactors and the IFR program. The EBR-II operational and fuel qualification data includes the irradiation of over 30,000 Mark-II driver fuel rods [3,4], 13,000 Mark-III/IIIA/IV (U–10Zr alloy) driver fuel rods, and over 600 U–Pu–Zr fuel rods [2,5] from 1964 to 1994 as well as the remote fabrication and irradiation in EBR-II of approximately 35,000 Mark-I driver fuel rods from 1964 to 1969 [6]. Mark-II driver fuel was qualified for 8 at.% burnup, while Mark-IIIA driver fuel was qualified for 10 at.% burnup. Mark-IIIA driver fuel was limited to 10 at.% due to swelling of the 316 stainless steel fuel assembly hardware. U–Pu–Zr and U–Zr rods clad in Type 316, D9 or HT9 cladding reached terminal burnup values of 15 to >19 at.% burnup without breach [6,7]. Some 2-sigma high-temperature assemblies reached 11–12 at.% burnup without breach [8]. In addition to EBR-II irradiations, over 1050 U–10Zr fuel rods and 37 U–Pu–Zr fuel rods were irradiated in the FFTF to burnup values above 14 at.% and 9 at.%, respectively [9] in order to qualify metal alloy fuel for FFTF core conversion. The significance of these irradiation tests were to: (1) effectively qualify U–Zr as the Series III.b driver fuel for FFTF (360 cm length), and (2) demonstrate that there were no metal fuel performance behaviors affected by fuel rod length that were obscured by the relatively short core height of EBR-II (34.3 cm length) [8]. The FFTF fuel design has a much higher aspect ratio (length/diameter) and the core environment creates a much larger peak-to-average fission rate.

An extensive review of historical US conventional fast reactor fuel technology with an expanded discussion of this information is provided by Crawford et al. [10]. Conventional fuel is defined

* Corresponding author. Tel.: +1 (208) 526 6360; fax: +1 (208) 526 0990.
E-mail address: Jon.Carmack@inl.gov (W.J. Carmack).

0022-3115/$ - see front matter © 2009 Elsevier B.V. All rights reserved.
doi:10.1016/j.jnucmat.2009.03.007

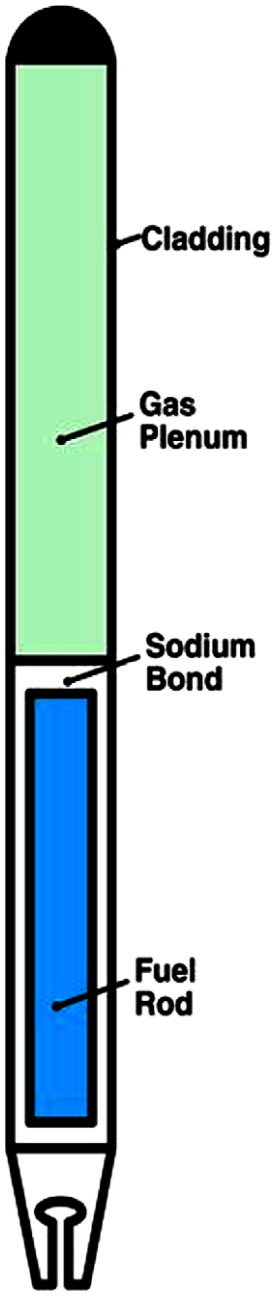

Fig. 1. Schematic of a metallic, sodium bonded, fast reactor fuel element.

as fuel forms that use highly enriched uranium (HEU) or U–Pu, that have been developed in domestic and international fast reactor programs. Features believed to be pertinent to transmutation fuel technology are summarized with the reader referred to the appropriate literature references for further detail.

Typically the fuel section of the metallic fuel element, as shown in Fig. 1, contains the fissile uranium, uranium–plutonium, or a mixture of uranium–plutonium and minor actinides. The fuel alloy is stabilized using typically a 10–30% addition of zirconium to both increase the melting point and to minimize fuel/cladding chemical interaction (FCCI). The fuel slug is thermally bonded to the cladding using sodium. The sodium provides a very high thermal conductivity medium by which heat is easily transferred to the cladding and reactor coolant. A fission gas collection plenum is provided to capture the released fission product gases. The fuel and sodium have typically been sealed inside a stainless steel cladding of austenitic or ferritic–martensitic (FM) composition or a nickel-based alloy. The current designs employ the low swelling FM stainless steels. Future designs may employ a FM steel in which a fine oxide powder has been dispersed to improve high-temperature strength and stress rupture properties.

Table 1 summarizes the experience with metal fuel compositions from the EBR-II metal driver fuel campaigns including general design parameters associated with the fuel campaigns. Future reactor fuel designs incorporate minor actinides/TRU (Pu, Am, Np, and Cm) obtained from spent light water reactor fuel into the fuel matrix. The objective is to destroy/burn the long-lived minor actinides (MA) and minimize long-lived radioactive waste. This fuel composition is referred to as the TRU bearing metal alloy. Table 2 provides the general design of the Global Nuclear Energy Partnership (GNEP) reference burner reactor fuel design and the burner and breakeven fuel designs for the Korea Atomic Energy Research Institute (KAERI)-sodium fast reactor (SFR) concepts. Both design concepts incorporate 20–30 wt.% transuranics into a fuel matrix of uranium and zirconium.

2. Materials and methods

2.1. Metallic fuel fabrication

As with metal alloy fuel performance, metallic fuel slug fabrication has progressed significantly since the first core loading of the EBR-I, termed the Mk-I fuel. Burkes et al. provide a detail synopsis of metallic alloy fuel fabrication history and techniques in an accompanying paper in these proceedings. The Mk-I fuel was unalloyed, highly enriched uranium metal that was rolled and swaged to the desired final shape. The second (Mk-II) and third core (Mk-III) loadings of EBR-I were centrifugally cast U–Zr alloy and centrifugally cast U–Zr alloy coextruded with Zircaloy-2 cladding, respectively. The fourth and final loading of EBR-I, Mk-IV, was a centrifugally cast, NaK-bonded Pu–Al alloy [1]. The first loading of EBR-II driver fuel was U-5Fs fabricated using fresh fuel and simulated fission products with equipment originally designed for remote use in a hot-cell [11]. Fs is designated the symbol for fissium. The nominal 5 wt.% Fs is a convenient abbreviation for the 2.4 wt.% Mo, 1.9 wt.% Ru, 0.3 wt.% Rh, 0.2 wt.% Pd, 0.1 wt.% Zr, and 0.01 wt.%

Table 1
Selected design parameters (nominal) of EBR-II metal driver fuel elements.

Campaign	Mark-I/-IA	Mark-II/-IIC/-IICS	Mark-III/-IIIA	Mark-IV	Mark-V/-VA[a]
Fuel alloy (wt.%)	U–5Fs	U–5Fs and U–10Zr	U–10Zr	U–10Zr	U–20Pu–10Zr
^{235}U enrichment (%)	52	67–78	66.9	69.6	Variable
Slug diameter (mm)	3.66	3.30	4.39	4.27	4.27–4.39
Fuel smeared density (%)	85	75	75	75	75
Burn up limit (at.%)	2.6	8.9	10	N/A	TBD
Plenum to fuel volume ratio	0.18	0.68-1.01	1.45	1.45	1.45
Plenum gas	Inert	Inert	Inert	Inert	Argon
Cladding material	SS 304L	SS304L and SS 316	CW 316 and CW D9	HT 9	HT 9 and CW 316

[a] Conversion to the Mark-V/-VA fuel types was not started before EBR-II was terminally shutdown in 1994.

Table 2
Selected design parameters of GNEP and KAERI–SFR metal fuel design concepts.

Design	GNEP (1000 MWth)	KAERI–SFR	
		Burner (800 MWth)	Breakeven (3000 MWth)
Fuel alloy (wt.%)	U-(~28 TRU)–10Zr	U-(22–30)TRU–10Zr	U-(15–17)TRU–10Zr
235U Enrichment (%)	Depleted	Depleted or recovered uranium	Depleted or recovered uranium
Slug diameter (mm)	6.03	4.4–6.0	6.30–6.77
Fuel smeared density (%)	75	60–75	75
Burn up limit (at.%)	13 nominal 19–20 advanced	13 average 17 peak	11 average 16 peak
Plenum to fuel volume ratio	2–2.5	1.75–2.5	1.75–2.5
Plenum gas	Inert	Inert	Inert
Cladding material	FMS, ODS	FMS	FMS

FMS, ferritic–martensitic steel.
ODS, oxide dispersion strengthened steel.

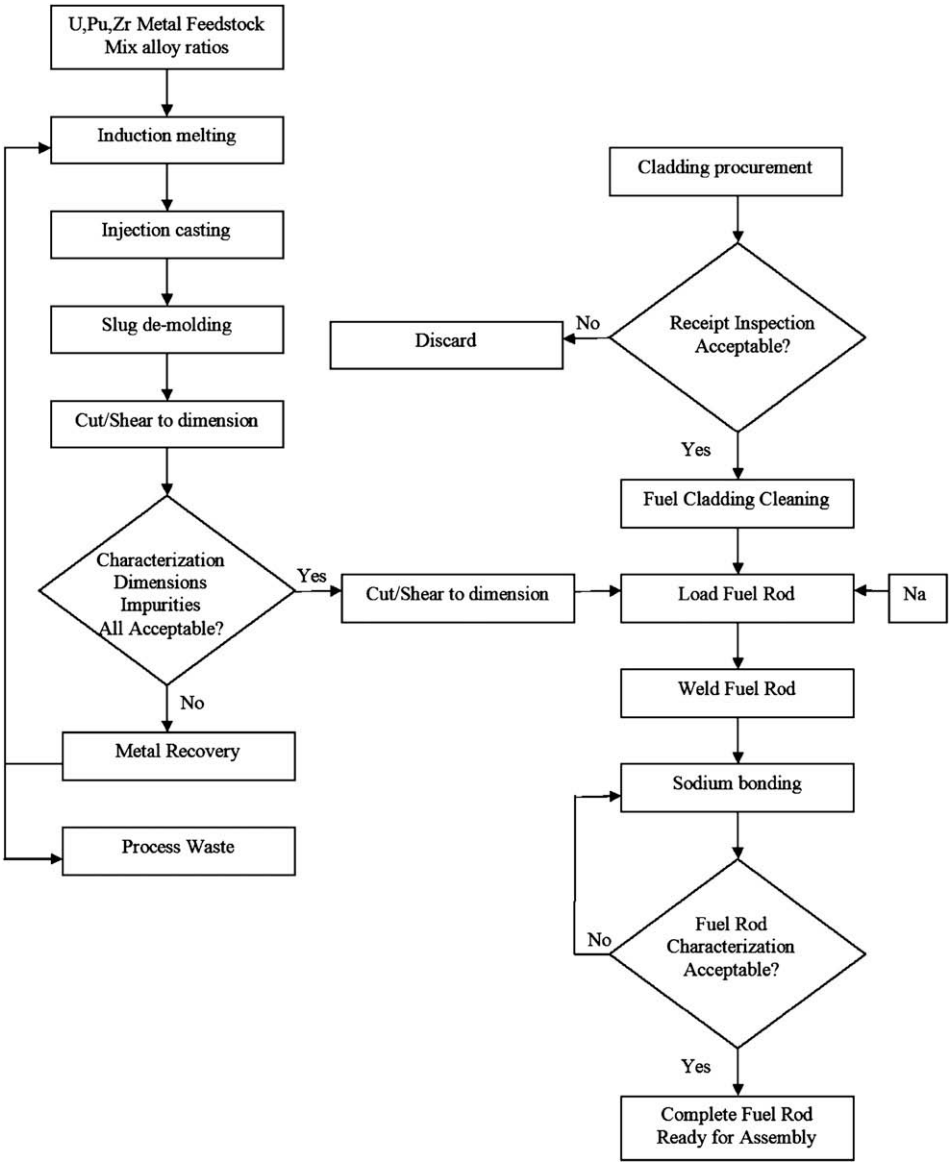

Fig. 2. Process flow diagram for fast reactor metal fuel fabrication.

Nb in the alloy. The U-5Fs alloy represented the equilibrium alloy for the melt refining process to be used for reprocessing irradiated nuclear fuel at that time [12]. Additional fabrication methods, such as wire drawing, powder metallurgy, and extrusion, were also considered. Each of these methods had process limitations resulting in a high degree of crystallographic texture requiring additional heat treatment.

Additionally, the fabrication equipment was complex and not favorable for remote use. Texturing of the fuel was undesirable since it promoted irradiation-growth-induced dimensional

changes that could cause cladding breach. Therefore, other fabrication methods were pursued.

A method capable of producing a fuel slug with a non-textured structure that required a relatively short fabrication sequence with easy-to-build, easy-to-use equipment was highly desirable. The fabrication technique with the most promise was precision injection casting that could be used in both a cold prototype line and a hot reprocessing-production line. The driver fuel for EBR-II and experimental fuels tested in both EBR-II and FFTF were fabricated using precision casting. A typical process flowsheet for precision cast fuel slugs is provided in Fig. 2.

2.2. Steady-state performance

Steady-state irradiation experience with metal fuel has established satisfactory performance and reliability of a plutonium fueled fast spectrum reactor [13], demonstrating burnup capability of up to 20 at.% under normal operating conditions [6,14–16], when clad with modified austenitic or ferritic–martensitic stainless steel alloys. Metal fuels with these characteristics have been shown to exhibit sufficient margin to failure under transient conditions for successful reactor operation [17–21]. Post-breach operation of metal fuel in a sodium cooled system is benign [4,22]. The irradiation performance of metal fuel is tied closely to the thermo-physical properties of the fuel alloy.

Metal fuel alloys have a propensity toward high gas-driven swelling. Features to restrain swelling axially were incorporated into early metal alloy fuel designs. This resulted in unacceptably large cladding deformation at low burnup as the swelling of the restrained fuel was then resolved radially and put stress on the cladding. Later designs allowed for this fuel swelling by increasing the fuel-cladding radial gap dimension. This configuration allows the fuel to freely swell about 30% by volume before contacting the cladding wall. At this point the fuel has developed a network of interconnected porosity, providing for easy gas release and resulting in a weak mass that cannot exert substantial mechanical force on the cladding. The network of porosity leads to a high gas release, approximately 80% of the fission gas produced. Since metal fuel is engineered to allow for swelling and promote gas release, large plenum-to-fuel volume ratios are used to prevent large plenum gas pressures. The TRU bearing metal alloy fuels also require the accommodation of gas generated from americium and curium transmutation and decay. Helium is the largest contributor to gas pressure arising from the transmutation of americium and subsequent decay of generated isotopes. The resulting pressurization can be controlled by sizing the fuel pin gas plenum to prevent excessive gas pressure driven cladding creep but this is not necessarily the desired option for advanced fuels and reactor systems.

Metallic fuel has demonstrated excellent steady-state irradiation performance characteristics. In addition to the 30 years of extensive irradiation experience with the driver fuel in EBR-II, extensive U–Zr and U–Pu–Zr irradiation tests have been conducted as part of the Integral Fast Reactor (IFR) Program [2,5]. A summary of metal fuel irradiation tests is provided in Crawford et al. [10] and Chang [23]. The IFR Program was initiated in 1984. A 10% zirconium addition, replacing the 5% fissium of previous EBR-II core loads, was selected as the reference alloying agent for both uranium and plutonium-bearing fuels. Earlier irradiation tests of various alloys indicated that Zr alloys exhibited exceptional compatibility with cladding in addition to significantly increasing the fuel alloy solidus and fuel-cladding eutectic temperatures. Therefore, as the Mark-II driver fuel assemblies reached their irradiation limits, the EBR-II core was gradually converted to new Mark-III fuel based on U–10%Zr with D-9 or 316 SS cladding. Later, Mark-IV fuel with HT-9 cladding was introduced. At the same time, the Experimental Fuels Laboratory (EFL) was established in 1984 to fabricate plutonium-bearing ternary fuel, U–xPu–10%Zr ($3\% \leqslant x \leqslant 28\%$). A total of 16,811 U–Zr and 660 U–Pu–Zr fuel pins were irradiated in EBR-II in the next 10 years until EBR-II was permanently shutdown at the end of September, 1994.

The irradiation behavior of the zirconium alloy metal fuel is very similar to that of the U-fissium. The fission gas pore morphology of the irradiated U-10Zr fuel is illustrated in Fig. 3. The dark areas are pores, which tend to become interconnected allowing fission gas release to the plenum. The U–Pu–Zr alloy fuel demonstrates a more complicated distribution of pore morphologies because they are dependent upon the phases present, and the ternary fuel has a much more complex set of phases [24]. Maintaining the fuel smeared density at or below 75% is required for the development of interconnected porosity. Experimental pins using 85% smear density were operated to over 10 at.% burnup without breach but the cladding strains were also larger for the fuel with the higher smeared density [25].

Driven by temperature gradients within the fuel, constituent (U, Pu, and Zr) redistribution occurs in the early stages of irradiation. Zones of relatively constant composition are formed, defined by operating temperatures which correspond to phase boundaries. This is especially prevalent in the ternary alloys. Based upon the location of phase field boundaries in the temperature gradient, zirconium tends to migrate to the center and the periphery, hottest or coldest areas [26,27], and uranium migrates in the opposite direction. Plutonium on the other hand tends to remain homogeneously distributed [26,27]. This is beneficial and tends to help the performance issues because Zr moves to the center raising the solidus temperature in the peak temperature region and to the periphery helping maintain the fuel-cladding compatibility. This radial zone formation occurs rapidly in the early stage of irradiation and it enhances the radial swelling markedly. This high rate of radial swelling in the hotter areas (phase fields) creates stresses in the cold areas (phase field near the periphery of the fuel). The stresses are large enough to result in some crack formation in the cold regions. The large cracks eventually get filled with swelling fuel as irradiation continues. The anisotropic swelling then results in much smaller axial growth of the ternary fuel compared to U–Fs or U–Zr fuels [5]. The axial growth of the uranium-based fuel is in the range of 8–10%, whereas it is in the range of 3–4% for the ternary fuel. Axial growth can be accommodated with fuel pin and core design.

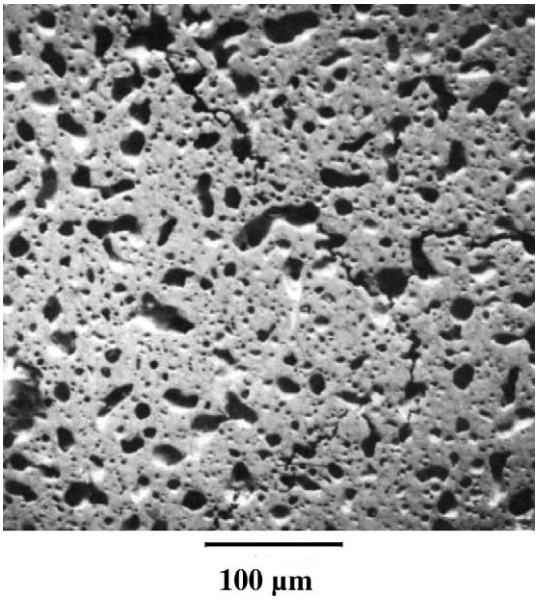

Fig. 3. Fission gas pore morphology in irradiated U–10Zr fuel.

The IFR Program test matrix included various combinations of cladding materials – austenitic stainless steel (316 SS), modified austenitic stainless steel (D-9), ferritic–martensitic (HT-9) steel, and modified ferritic–martensitic (HT-9 M) steels. Other variables included pin diameters ranging from 4.4 to 12.9 mm, plutonium concentrations (nominally 3%, 8%, 19%, 26%, 28.5%), Zr contents (2%, 6%, 10%, and 12%), fuel smeared densities (70%, 75%, and 85%), fabrication variables (fuel impurity levels and Na-bond defects), and operating conditions (peak linear power, cladding temperatures, etc.). Typically, the test assemblies were reconstituted after selected pins were removed and replaced to allow post-irradiation examinations at various burnup levels.

There is a perception that the excellent performance experience of the metal fuel in EBR-II was due to a small pin size (4.4 mm diameter and 34.3 cm length), and there is a concern whether the metallic fuel can perform as well in full length pin expected in commercial fast reactors. However, the fuel length effects were satisfactorily resolved in the Fast Flux Test Facility (FFTF) tests designated IFR-1, and the MFF series with 360 cm length fuel pins. The IFR-1 assembly contained U-(8 or 19)Pu–10Zr fuel pins, which achieved a peak burnup of 10.2%. The MFF fuel tests included six full assemblies and two partial assemblies of metallic fuel irradiated in FFTF. They were part of the FFTF core conversion qualification tests of U–Zr fuel with HT-9 cladding, the Series III.b design [28]. All of these assemblies achieved peak burnup in excess of 10% and the lead test achieved a peak burnup of 16% without a breach. The FFTF core conversion with metallic fuel was abandoned when a decision was made to shutdown FFTF in 1994.

Potential performance issues include the effect of height and weight of a long fuel column on fission gas release, fuel swelling characteristics, and potential fuel-cladding mechanical interaction in the lower part of the fuel column. The post-irradiation examinations of the FFTF tests indicated that the fission gas release to plenum was comparable to the EBR-II fuel, there was no difference in constituent migration, axial growth was as predicted, and there was no evidence of enhanced fuel-cladding mechanical interaction. There is a potential advantage to the longer fuel column in that most related core designs produce a larger peak-to-average fission rate so that the maximum burnup and maximum cladding temperature occur in different axial locations along the fuel pin, the former at core centerline and the latter at the top of the fuel column. Because rare earth fission products and temperature are important components in deleterious fuel-cladding chemical interaction, the fact that peak burnup and peak cladding temperature do not occur at the same location is a potential advantage.

2.3. High burnup capability

The burnup potential of metal alloy fuel was well demonstrated in the binary and ternary fuel compositions during the EBR-II and FFTF driver fuel and experimental programs to approximately 10 at.% burnup as discussed above. Higher burnups were also demonstrated during the fuel development programs of the 1990s. When EBR-II operation was ended on September 30, 1994 a number of fuel experiment assemblies were still under irradiation. The burnup values achieved in these test assemblies were significant. For example, the X425 lead test with U–Pu–Zr ternary fuel achieved 19.3% burnup and the X435 Mk-III driver qualification test achieved 19.9% burnup at the time of EBR-II shutdown. At the time, there was no indication that these tests needed to be terminated and much higher burnup levels could have been achieved if irradiation continued. Post-irradiation examination of the X435 and X425 experiments were conducted but not published in open literature. It is expected that summaries of these experiments and the post irradiation examination results will be published in the near future.

There is no indication in minor actinide bearing metal fuels that high burnup values cannot be achieved but three key phenomena are known to present challenges to fuel integrity at high burnup. Similar to binary and ternary metal fuel alloys, minor actinide bearing fuel systems will still be dependant upon the integrity of the cladding. At high burnup, high fission gas pressures are realized; the creep strain and strain rate increase, and neutron damage to the cladding increases the cladding susceptibility to failure. Dose tolerant cladding will be needed for high burnup. Also similar to binary and ternary fuel compositions, minor actinide bearing fuel at high burnup may exhibit fuel constituent redistribution possibly leading to fuel-cladding chemical interaction. Future advanced claddings may provide the solution to all three issues, with low fuel-cladding chemical interaction potential as well as having high strength and dose tolerance.

2.4. Minor actinide (MA) bearing metallic alloy fuels behavior

Metal fuel provides the potential for excellent performance as a MA-bearing fuel considering the demonstrated performance of conventional metal fuels. Study of these issues forms the basis for defining the current focus areas of metal MA-bearing fuel research and development:

- Demonstration of MA-bearing feedstock reduction to metal alloy feedstock. It is expected that the MA-bearing feedstock available for fuel fabrication will be in oxide form. This feedstock must be reduced to metal for metal alloy fuel fabrication.
- Due to Am metal volatility, fabrication with high Am retention must be demonstrated using revised casting technology utilizing higher pressure systems, shorter heating times, and removing conditions that would promote Am vapor deposition.
- Metal fuel properties must not be seriously degraded as compared to the U, Pu, Zr system performance by the addition of the MAs (Am, Np, and Cm).
- Demonstration of an acceptable level of fuel-cladding-chemical-interaction (FCCI) with fuel that includes rare earth impurities and MA fuel constituents over the lifetime of the fuel up to its burnup limit, ~20 at.%.
- Assuming fuel melting and FCCI characteristics are acceptable; behavior of MA-bearing fuel in over-power transients and run beyond cladding breach should be acceptable as well. Performance modeling and perhaps proof testing of these assumptions may be required.
- Burnup limitation extensions to greater than 23 at.% (at 39×10^{22} n/cm^2 or approximately 200 dpa) can be anticipated with current ferritic/martensitic steel cladding and up to 30 at.% may be achievable with increased high-temperature cladding strength and performance [13].

An important question related to the use of U–Pu–Am–Np–Cm–Zr alloys as transmutation fuels are the unknown phase equilibria in the multi-component alloy system. The potential for immiscibility and formation of an inhomogeneous microstructure is not a fuel performance issue, as shown by the excellent performance of multi-phase U–Pu–Zr fuel [4]. Rather, the formation of low melting phases in the complex alloy system is an issue that must be experimentally determined. Recent experimental irradiations and out-of-pile studies conducted as part of the AFCI program indicate that this is not an issue [29].

Recycling technology for metal fuel by pyroprocessing has been established by pyroprocessing on an engineering scale. Remote fabrication was established as part of the EBR-II development program in the 1960s with the remote fabrication of more than 39,000 fuel pins in the Fuel Cycle Facility in Idaho.

Three steady-state transuranic metal fuel tests have been conducted, EBRII-X501, AFC1, and METAPHIX-1 and -2. The issues relevant to TRU metal alloy fuel fabrication and irradiation performance known from these experiments are presented below. Current irradiation experiments include the AFC2 series, conducted in flux filtered tests in the Advanced Test Reactor, as well as METAPHIX-3 and the FUTURIX–FTA series, both conducted in the fast spectrum Phenix test reactor.

3. Results

3.1. X501 U–Pu–Zr–Am–Np metal fuel experiment

The X501 experiment was conducted in EBR-II as part of the IFR (Integral Fast Reactor) program to demonstrate minor actinide burning through the use of a homogeneous recycle scheme. The X501 subassembly contained two metallic fuel elements, based upon U–20Pu–10Zr and loaded with 1.2 wt.% americium and 1.3 wt.% neptunium. Fuel slugs were fabricated by using differential pressure injection casting. Details of the casting process and resulting microstructure are given in Ref. [30]. Considerable americium was lost during the fabrication process. The presence of Ca and Mg in the Am feed material created an effervescence upon addition to the melt and certainly was the reason for much of the loss. The amount lost as a result of the high vapor pressure of Am is unknown. However, surrogate testing using a U–Mn–Zr melt (Mn having approximately the same vapor pressure as Am) indicated that the high vapor pressure solute could be retained. Moreover, modeling of the expected loss of Am as a vapor also indicates that control of the casting design and conditions should allow losses to be minimal.

The X501 subassembly was inserted into EBR-II beginning in February 1993, and withdrawn just prior to EBR-II shutdown in August 1994 for a total irradiation time of 339 EFPDs. Burnup, calculated on the basis of REBUS/RCT/ORIGEN [30] was 7.6% HM with transmutation of 9.1% of ^{241}Am. Peak linear heat generation rate was estimated to be 45 kW/m (13.7 kW/ft) and peak fuel centerline and cladding inner surface temperatures were approximately 700 and 540 °C, respectively.

A partial post-irradiation examination was completed on X501, including gamma scanning, optical microscopy, microprobe analysis, and metallography. A microscopic examination of the inside cladding surface was made to determine if the inclusion of the MAs in U–Pu–Zr fuel has an effect on FCCI (Fuel-Cladding Chemical Interaction). The HT-9 cladding used for the X501 experiment is also the reference cladding for US transmutation fuel. Optical microscopy showed no evidence of reaction layer formation on the inner cladding wall or the outer surface of the fuel slug. A gap is visible between the fuel and the cladding wall at all locations. These preliminary results indicate that under typical metal fuel operating conditions, FCCI of HT-9 is not strongly affected by small amounts of americium or neptunium. The irradiated fuel showed a microstructure where constituent radial redistribution resulted in the formation of three microstructural zones within the fuel, typical of U–Pu–Zr fuels [26,27]. The X501 experiment demonstrated the acceptable behavior of U–Pu–Zr fuel with small but significant additions of americium and neptunium to intermediate burnup.

3.2. AFC-1/ATW/FUTURIX–FTA

A number of TRU bearing metal fuel compositions containing various quantities of U–Pu–Zr, and MAs have been tested in HT-9 cladding in the Advanced Test Reactor as part of the ATW and AFC-1 series of irradiations under the AFCI program, a series of cadmium shrouded and flux filtered capsule experiments [31]. All of the metal fuel compositions have shown excellent performance up to 8–10 at.% burnup. Behavior typical of the ternary U–Pu–Zr alloy system has been observed with no fuel failures and no unexpected fuel performance issues identified [31].

In conjunction with the AFC test series, a series of test compositions shown in Table 3 was placed in the fast spectrum Phenix reactor in May of 2007 as part of the FUTURIX–FTA irradiation. Table 4 provides a summary of the metal alloy compositions studied during the AFC-1 test series. Fig. 4 shows a photomicrograph of the AFC-1 (U-29Pu–4Am–2Np–30Zr) composition at approximately 6 at.% burnup [31,32]. Development of microstructure characteristic of metal fuels will develop at higher fission density than that exhibited in the low density-low burnup actinide bearing fuel shown in Fig. 4.

3.3. METAPHIX

The METAPHIX set of experiments is being conducted as a collaboration between the Central Research Institute of Electric Power Industry (CRIEPI) and the Institute for Transuranium Elements (ITU) with support from of Commissariat a l'Energie Atomique (CEA) in the Phenix fast test reactor located in France. It consists of U–Pu–Zr metal fuel base compositions containing transuranics and rare earths. This experiment will provide substantial data on

Table 3
Summary of test compositions in FUTURIX–FTA.

Non-fertile fuels	Low-fertile fuels
48Pu–12Am–40Zr	(35)U–29Pu–4Am–2Np–30Zr
(Pu0.50, Am0.50)N + 36 wt.% ZrN	(U0.50, Pu0.25, Am0.15, Np0.10)N
(Pu0.20, Am0.80)O2 + 65 vol.% MgO	
(Pu0.50, Am0.50)O_2 + 70 vol.% MgO	
(Pu0.23, Am0.25, Zr0.52)O_2 + 60 vol.% Mo92	
(Pu0.50, Am0.50)O_2 + 60 vol.% Mo92	

Table 4
Summary of test compositions in AFC-1 series.

AFC1-B, D Non-fertile (~83% 239Pu)	AFC1-F, H Low fertile (~83% 239Pu)
40Pu–60Zr	35U–29Pu–4Am–2Np–30Zr (78% 235U)
60Pu–40Zr	30U–25Pu–3Am–2Np–40Zr (93% 235U)
50Pu–10Np–40Zr	40U–34Pu–4Am–2Np–20Zr (33% 235U)
48Pu–12Am–40Zr	35U–28Pu–7Am–30Zr (93% 235U)
40Pu–10Am–10Np–40Zr	

Fig. 4. Cross-sectional photomicrograph AFC-1F Composition A1F4 (U–29Pu–4Am–2Np–30Zr) irradiated to 6.8 × 10^{20} fissions/cm^3 (approximately 6.0 at.%).

the performance of TRU metal fuels containing rare earths under fast reactor irradiation conditions. There are three assemblies (METAPHIX-1, 2, and 3) irradiated to burnups of ~2.5, ~7, and ~11 at.%, respectively. The first two were discharged from the Phenix reactor in August 2004, and in July 2007 and some examinations have been performed [33] METAPHIX-3 is scheduled to be discharged in April of 2008. There have been no fuel failures observed [34].

3.4. AFC-2

The AFC-2 test series is an experiment that is currently being conducted in the ATR in similar conditions and geometries to the AFC1 and ATW test series. Table 5 provides a summary of the compositions currently under irradiation. The AFC2 tests provide a similar alloy mix as the AFC-1 tests but conducted to much higher burnup levels of 10–20 at.%.

3.5. Metallic fuel transient overpower capability

Safety testing established the acceptable behavior of metal fuel during accident conditions. Assessment of safety of an operating fast reactor requires an understanding of how fuel rods and bundles behave under off-normal conditions. The six M-series tests performed in the Transient Reactor Test Facility (TREAT) evaluated transient overpower margin to failure, pre-failure axial fuel expansion, and post-failure fuel and coolant behavior for 15 rods with various combinations of U-5Fs, U–Zr, and U–Pu–Zr fuel clad in Type 316, D9, and HT9 stainless steels [4,17]. The results consistently showed that metal fuel rods of modern design exhibited failure thresholds ~4 times nominal power (under the relatively fast transient overpower conditions used in the tests). Fuel rod breaches that occurred were located at the top of the fuel column and in all cases were attributed to cladding rupture induced by stresses created by plenum pressurization and enhanced by cladding thinning caused by eutectic-like formation of a molten fuel/cladding phase that penetrated the cladding wall. Pre-failure axial fuel expansion (which has the beneficial effect of removing reactivity from the core during an overpower transient) for the U–Pu–Zr and U–Zr was similar to that observed with higher burnup U–5Fs fuel [17], and in amounts significantly greater than would be caused by thermal expansion alone. Post-failure behavior observed in all tests was characterized by rapid fuel dispersal, with about half of the fuel inventory being ejected from the fuel rod – again, with the beneficial effect of removing reactivity from the core during postulated severe accidents. The data from these tests and from a large number of prior metal fuel transient tests in TREAT were used to develop and validate models of fuel behavior under transient overpower conditions [35,36].

3.6. Metallic fuel safety performance

Other safety-related testing of metallic fuels has focused on fuel behavior during unlikely loss-of-flow events, using hot-cell furnace heating tests of irradiated U–Pu–Zr clad in HT9 [19,37]. The results demonstrated significant safety margin for the particular transient conditions studied (a bounding unlikely loss-of-flow event for EBR-II). The observed cladding breaches were induced stress imposed on the cladding due to pin-plenum gas pressure at temperature and enhanced by cladding thinning caused by eutectic-like formation of a molten fuel/cladding phase. In addition, fission gas expansion in the fuel induced axial fuel expansion, enabled by reduction of constraint from the cladding with formation of the molten phase at the fuel/cladding interface. The data from these tests, and other similar tests, were used to develop and validate models of fuel behavior under loss-of-flow conditions [36,37].

Metal fuel has excellent transient capabilities and does not impose any restrictions on transient operations or load-following capabilities. The robustness of metal fuel is illustrated by the following history of typical driver fuel irradiated during the EBR-II inherent passive safety tests conducted in 1986 [17]:

- 40 start-ups and shutdowns
- 5–15% overpower transients
- 3–60% overpower transients
- 45 loss-of-flow (LOF) and loss-of-heat-sink tests including a LOF test from 100% power without scram.

Metal fuel also has benign run beyond cladding breach (RBCB) performance characteristics. A cross-section of a metal fuel pin (12 at.% burnup) used in an RBCB test is illustrated in Fig. 5. Note that the cladding wall had been thinned to induce cladding failure early in the test. Because metal fuel is compatible with sodium, there is no reaction product and the fuel loss is practically zero. The post-irradiation examination shown in Fig. 5 is after operation in RBCB mode for 169 days and there is no indication of breach site enlargement. In another test, metal fuel operated 223 days beyond cladding breach, including many start-up and shutdown transients, and the breach site remained small. Metal fuel is expected to be very reliable. However, even if unforeseen fuel failure occurs, the failed fuel pins could be left in the core until the expected end of life without raising any operational or safety concerns.

The eutectic formation temperature between the fuel and the cladding has been considered a critical parameter for the metal fuel pin design. The onset of fuel-cladding eutectic formation starts in the 650–725 °C range, depending on the fuel alloy and cladding

Table 5
AFC-2A and AFC-2B fuel test matrix.

Rodlet	Metallic fuel alloy[a]
1	U–20Pu–3Am–2Np–15Zr
2	U–20Pu–3Am–2Np–0.8RE[b]–15Zr
3	U–20Pu–3Am–2Np–1.5Re[b]–15Zr
4	U–30Pu–5Am–3Np–1.5Re[b]–20Zr
5	U–30Pu–5Am–3Np–0.8RE[b]–20Zr
6	U–30Pu–5Am–3Np–20Zr

[a] Alloy composition expressed in weight percent.
[b] RE designates rare earth alloy (16% La, 53% Nd, 31% Ce).

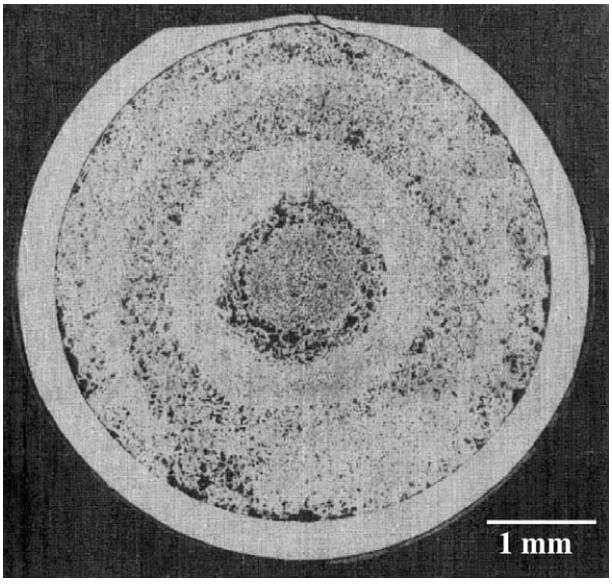

Fig. 5. Example of RBCB test of metal fuel.

types. However, at this onset temperature, not much interaction occurs. In fact, even at 100 °C above the eutectic temperature, the eutectic penetration into the cladding is minimal in 1 h, although a significant fraction of the fuel may partially liquefy. Only at much higher temperatures, close to the fuel melting point itself, does the eutectic penetration into cladding become rapid. Therefore, the eutectic formation is not a primary safety concern during transient overpower conditions. However, the eutectic temperature limits the coolant outlet temperature to 500–510 °C in order to provide adequate margins to onset of eutectic formation. Note that a cladding liner that prevents fuel/cladding interaction, such as zirconium or vanadium, could be used to mitigate this limitation.

It is difficult to raise the fuel temperature of metal alloy fuel because of the high thermal conductivity (~20 W/m-K). As a result, operating margins in terms of power can, in fact, be greater for the metal core than other fuel systems. Metal fuel provides better or equal safety characteristics across the entire spectrum from normal behavior to postulated severe accidents. However, it is in the inherent passive safety characteristics under the generic anticipated transient without scram events, such as loss-of-flow without scram (LOFWS), loss-of-heat-sink without scram (LOHSWS), and transient overpower without scram (TOPWS), that the metal fuel shows its excellent advantages.

The inherent passive safety potential of the metal fuel was demonstrated by two landmark tests conducted in EBR-II on April 3, 1986 [38,39] These tests, LOFWS and LOHSWS, demonstrated that the unique combination of the high heat conductivity of metal fuel and the thermal inertia of the large sodium pool can shut the reactor down during these potentially very severe accident situations, without depending on human intervention or the operation of active, engineered components. The LOFWS event can be initiated by station blackout. Nuclear power plants have redundant power supply sources and even if the alternate line is also disabled, then an emergency power supply system on-site will be activated. Should this also fail, the plant protection system will automatically shut the reactor down. Of course, the plant protection system has redundancy – if the primary shutdown system fails, then the secondary shutdown system will be activated. If this fails, the operator can manually shut the reactor down. The LOFWS test in EBR-II simulated an ultimate scenario where all of the above safety systems and operator actions had failed [40].

As the power to the primary pump is lost, the coolant flow is reduced rapidly while the reactor is at its full power. This then causes the reactor coolant outlet temperature to rise very rapidly (about 200 °C in 30 s). This rising coolant temperature then causes the heatup and thermal expansion of the core components, in particular the fuel assembly hardware, which enhances the neutron leakages and hence slowing down the nuclear chain reaction. Due to this negative reactivity feedback, the reactor power is shutdown all by itself and the coolant temperature rise stops, eventually brought to an asymptotic temperature at equilibrium with the natural heat loss from the system. It should be pointed out that during the initial tens of seconds, the mechanical pump inertia provided a flow coastdown avoiding immediate local sodium boiling and enabling a gradual transition to natural convection flow through the core.

Following the LOFWS test, the LOHSWS test was conducted on the same day. The loss-of heat-sink was initiated by the shutdown of the intermediate pump, which isolated the primary system, while the primary pump was functioning to remove the heat from the core to the primary tank. The intermediate loop flow is reduced to zero, which disables the normal heat-sink in the balance of plant. The core heat is dumped to the entire inventory of the primary sodium, which raises the core inlet temperature. This is a rather slow transient and it took about 10 min to raise the primary sodium temperature by about 40 °C. This gradual increase in the reactor inlet temperature has the same effect – thermal expansion and enhanced neutron leakages – and the power is reduced. And the reactor outlet temperature is reduced accordingly.

These remarkable inherently passive benign responses to the most severe accident scenarios are unique to the metal fueled fast reactor due to the combination of the following three factors: Sodium coolant with large margins to boiling temperature, pool configuration with large thermal inertia, and metal fuel with low stored Doppler reactivity. The first point is obvious to ride out the initial coolant temperature rise. The second point is necessary to provide time for thermal expansion of heavy structures to take place and is dependant upon reactor plant configuration. The third point on metallic fuel is not so obvious and requires some explanation. The characteristics of the negative reactivity feedback caused by the increase in coolant temperature determine the reactor response. The most important factor differentiating the responses in metal and oxide fuels is the difference in stored Doppler reactivity between the two fuel types. As the power is reduced, the stored Doppler reactivity comes back as a positive contribution, tending to cancel the negative feedback due to the structural expansion. The high thermal conductivity of metal fuel and consequent low fuel operating temperature give a stored Doppler reactivity that is only a small fraction of overall negative reactivity feedback. As a result, the power is reduced rapidly.

The neutronics performance characteristics of metallic fuel allow core designs with minimum burnup reactivity swing even for small modular designs. This can be used not only in extending core life to 30 years but also in reducing the TOPWS initiator caused by an unprotected control rod runout. Transient overpower tests on metallic fuels performed in TREAT have demonstrated a large margin to cladding failure threshold for the metallic fuel. Another significant finding from these TREAT tests is that fission gas-driven axial expansion of fuel within the cladding before failure provides an intrinsic and favorable negative reactivity feedback in the metallic fuel that has no parallel in other fuel systems. The metallic fuel pre-failure axial extrusion as a function of burnup is illustrated in Fig. 6.

3.7. Metallic fuel properties

Material properties define the behavior and performance of metal alloy fuels. Table 6 provides a summary of fuel material properties for U–20Pu–10Zr, after Smith et al. [41]. In the following

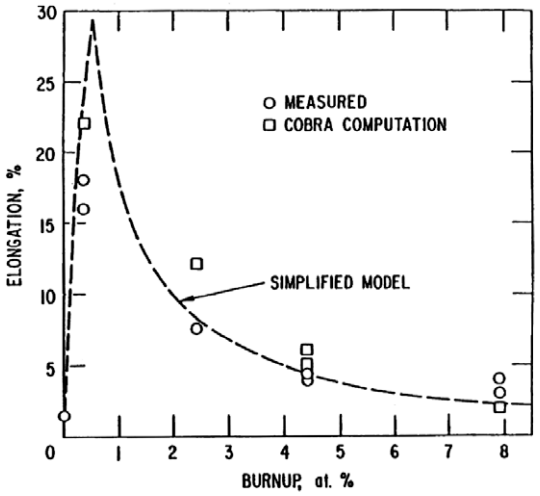

Fig. 6. Axial pre-failure fuel extrusion as a function of burnup.

Table 6
Selected metal fuel material properties.

Fast reactor fuel type fresh fuel properties	Metal (U–20Pu–10Zr)
Heavy metal density (g/cm3)	14.1–14.3
Melting point (°C)	1077
Thermal conductivity (W/m K)	16
Operating centerline temperature at 40 kW/m, °C (T/Tmelt)	787 (0.8)
Fuel-cladding solidus (°C)	662
Thermal expansion (l/°C)	17E-6
Heat capacity (J/g °C)	17
Enthalpy (kJ/mol)	30
Sodium compatibility	Compatible
Fuel-cladding interaction	Some corrosion/cladding wastage created by rare earth and fission product interdiffusion with cladding – could be mitigated with a cladding liner
Pu enrichment capability	No limit by phase instability. Higher enrichment lowers eutectic temperature
Steady state irradiation	
Burnup	200 GWd/t
Cladding temperature	<600 °C
Linear power (driver)	<450 W/cm
Linear power (test)	<600 W/cm
FP gas release	~85%
Clad corrosion	~ 170 μm max at 640 °C, 100 GWd/t
FCMI	Insignificant in lower smear density fuel
Cladding breach	Expected mechanism is creep rupture due to gas pressurization
Transient tests	6

section, the physical properties, mechanical properties, and behavior laws and correlations of metal alloy fuel will be presented.

3.7.1. Physical properties

3.7.1.1. Melting temperature. Solidus temperatures for the metallic alloys to be irradiated have not yet been determined experimentally. Assessed binary phase diagrams with limited experimental data for Pu–Zr, Pu–Am and Pu–Np are presented in the subsequent section on 'Phase Diagrams'. Plutonium is the lowest-melting element among Pu, Am, Np and Zr at 640 °C, with Np close at 645 °C. Alloying Pu with either Am or Zr serves to increase the solidus temperature significantly, while alloying Pu with Np only slightly affects the solidus temperature. Pu–40Zr has a solidus temperature of over 1230 °C. Therefore, until an experimental determination of the solidus temperatures of Pu–Am–Np alloyed with 40 wt.% Zr has been determined, 1230 °C will be used as an estimate of the solidus temperature.

3.7.1.2. Thermal conductivity. The thermal conductivities of the Pu–Am–Np–Zr alloys have not yet been measured. Fig. 7 provides a graphical representation of the estimate of the thermal conductivity for Pu–40Zr obtained using Pu and Zr elemental thermal conductivities and an analytical alloy model [42]; note that the binary alloy undergoes a phase change from δ-Pu to ε-Pu at about 600 °C which gives rise to a discontinuity in the thermal conductivity. Since Am and Np have thermal conductivities similar to Pu, it is recommended that the Pu–40Zr data be used for all the Pu–Am–Np–40Zr alloys until experimental measurements can be made.

The average thermal conductivity of metal fuel is high (~16 W/m K) resulting in a low centerline operating temperature, approximately 790 °C at 40 kW/m linear heat rate.

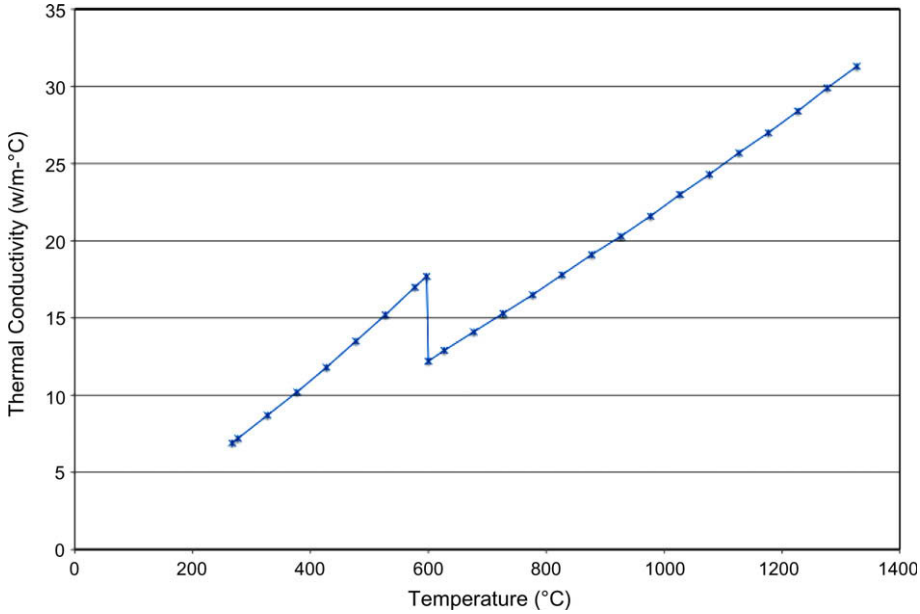

Fig. 7. Estimated thermal conductivity of Pu–40Zr.

3.7.1.3. Specific heat. The specific heat of the Pu–Am–Np–Zr alloys is estimated using the Kopp–Neumann law which weights the elemental specific heats with their corresponding constituent mole fraction in the alloy to obtain the alloy specific heat. Fig. 8 provides a graphical representation of the specific heat of U–Pu–Am–Np–Zr alloy.

3.7.1.4. Thermal expansion. No data is available for the alloys of interest, nor for Pu–Zr alloys. The thermal expansion coefficient for U–15Pu–10Zr is $17.6 \times 10^{-6}\,K^{-1}$ for $298 < T \leqslant 900$ K, and $20.1 \times 10^{-6}\,K^{-1}$ for $T > 900$ K [43,44]. The thermal expansion coefficient for pure Pu is $15.0 \times 10^{-6}\,K^{-1}$ for $T > 763$ K.

3.7.1.5. Density. Experimental measurements for the densities of these metallic alloys have not yet been made. The theoretical densities have been estimated by summing the elemental densities for the anticipated phases weighted by their mole fraction in the alloy as 9.77 g/cm^3 for the Pu–12Am–5Np–40Zr alloy and 9.39 g/cm^3 for the Pu–48Am–5Np–40Zr alloy. These fuel alloys will have no porosity on fabrication.

3.7.2. Mechanical properties

Mechanical properties/behavior of low smear density metallic fuel does not contribute significantly to its performance. This is due to the fact that the large fuel-cladding gap allows the unrestrained swelling of the metallic fuel to occur to the point where fission gas porosity becomes interconnected, resulting in the release of most of the fission gases being produced and eliminating the major driving force for continued swelling. Fuel-cladding mechanical interaction (FCMI) occurs due to solid fission product accumulation/swelling only at very high burnup (e.g., 15–20 at.%); even then, the porous fuel has little rigidity. Thus, FCMI is at most a lower order effect in metallic fuel pins and is not an anticipated cause for failure.

3.7.2.1. Young's modulus. No data exists for the Young's modulus of Pu or Am alloys. The Young's modulus for pure plutonium is 107 GPa at room temperature (α-Pu) [44].

3.7.2.2. Poisson's ratio. No data exists for Poisson's ratio of Pu or Am alloys. The Poisson's ratio for pure plutonium is 0.15–0.21 at room temperature (α-Pu) [44].

3.7.2.3. Yield stress. Little data exists for the yield strength of Pu or Am alloys. The room temperature yield strengths for pure uranium and plutonium are 240 and 300 MPa, respectively [44].

3.7.2.4. Ultimate tensile stress. Little data exists for the ultimate tensile strength of Pu or Am alloys. However, pure Pu is relatively soft at temperatures approaching 100 °C and above, and additions of even small amounts of Zr greatly increase the strength at these moderate temperatures. For example, at 180 °C the ultimate strength of Pu is ~20 MPa, while an addition of 2.4 at.% (0.9 wt%) increases the strength to 125 MPa [45]. The ultimate tensile strength for pure uranium and plutonium at room temperature are 585 and 525 MPa, respectively [44].

3.8. Behavior laws

3.8.1. Irradiation swelling

Metallic alloy fuels of low smear density swell rapidly to approximately 30%, at which time the porosity being generated becomes interconnected. Once this network of interconnected porosity develops, most of the fission gases being produced are released and gas-driven fuel swelling falls off dramatically. Subsequent to this fuel swelling is primarily via solid fission product accumulation [4]. This behavior can be described as:

$$\Delta V/V = 150 \bullet B, \quad \text{for } B \leq 0.02$$
$$\Delta V/V = 0.30 + 0.5 \bullet B, \quad \text{for } B > 0.02$$

where $\Delta V/V$ is fuel swelling and B is the burnup expressed as a fraction of initial heavy metal.

3.8.2. Creep

The creep rate of the alloys of interest has not been measured. The recommended creep rate correlation for U–Zr and U–Pu–Zr alloys is [46]:

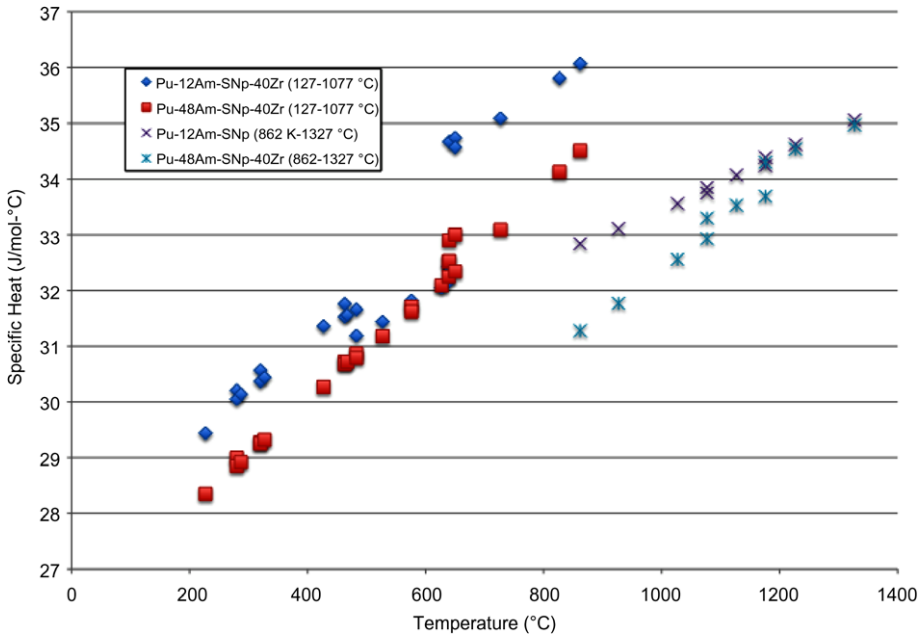

Fig. 8. Specific heats of metallic U–Pu–TRU alloys.

$$\varepsilon' = 5.0 \times 10^3 \bullet (1 + 7.9 \bullet P + 470 \bullet P^2) \bullet \sigma \bullet \exp\{-52,000/RT\} + 6.0 \bullet (1 - P^{2/3})^{-4/5} \bullet \sigma^{4.5} \exp\{-52,000/RT\} + 7.7 \times 10^{-23} \bullet \sigma \bullet F,$$

Where ε' is the steady-state creep rate (s^{-1}), P is porosity expressed as a fraction of initial fuel volume, R is the gas constant (1.987 cal/mol K), σ is stress (MPa), T is temperature (K), and F is the fission rate (fissions/cm^3 s).

3.9. Physics models

3.9.1. Gas release

A wide variety of metallic alloy fuels of low smear density have been observed to exhibit essentially the same fission gas release behavior [4]. This behavior can be described as:

$$\text{FGR}k = 40.0 \bullet B, \quad \text{for } B \le 0.02$$
$$\text{FGR} = 0.8, \quad \text{for } B > 0.02$$

where FGR is the fraction of total fission gases generated that is released from the fuel, and B is the burnup expressed as a fraction of initial heavy metal. For conservatism, it should be assumed that all helium produced in the fuel is released.

3.9.2. Densification

Densification does not occur for metallic fuel since it is fabricated with essentially no porosity.

3.10. Phase and chemical compatibility

3.10.1. Phase diagrams

No ternary phase diagrams exist for the systems of interest. Evaluated phase diagrams for Pu–Zr, Am–Pu and Np–Pu can be found in Kassner and Peterson [47]. Limiting fuel temperature (i.e., solidus temperature) was discussed above in the section on 'Melting Temperature'.

Phase diagrams do not exist for Fe–Np and Am–Fe; Fig. 9 gives the Fe–Pu phase diagram [47]. Since Pu is one of the constituents that attacks stainless steel cladding (FCCI) in metallic fuels, concern has been raised regarding the possibility of forming phases that melt at low temperature (e.g., Fe–Pu eutectic at 430 °C). However, extensive annealing studies conducted on diffusion couples between Pu-bearing metallic fuels and stainless steel cladding has never show melting at the Fe–Pu eutectic temperature. The minimum melting temperatures observed for U–26Pu–10Zr/stainless steel diffusion couples annealed for a minimum of 300 h were found to be 650 °C for either HT-9 (ferritic–martensitic) or D-9 (austenitic) steels and 775 °C for 316SS [4].

3.10.2. Chemical compatibility

Metallic fuel alloys containing U, Pu, Am, Np and Zr were fabricated with a sodium bond and both austenitic and ferritic–martensitic stainless steel cladding and irradiated in EBR-II over years. These alloys are completely compatible with the sodium used as a liquid metal bond and reactor coolant, exhibiting no reaction [4]. Fuel-cladding chemical interaction between these Zr-based fuel alloys and the stainless steel cladding has been observed to occur at a relatively predictable rate [48]. For austenitic stainless steels, FCCI is described by the correlation [49]:

$$L = A \bullet (t - 158) \bullet \exp\{Q/RT\},$$

where L is the depth of cladding penetration (mils, or thousandths of an inch); A is the constant 1.718×10^{11}; t is irradiation time (days); Q is the activation energy (49,461 cal/mol); R is the gas constant (1.987 cal/mol K); and T is the peak inner cladding temperature (K). Because the FCCI involves interdiffusion of rare earth fission products and cladding components, the above equation could be enhanced for reprocessed fuel with rare earth fission product carryover. This depends on the contributions to rate control of the diffusion process versus the supply of rare earths. Note that both the FCCI and 'eutectic'-like formation during transients can be mitigated with the use of a cladding liner that prevents fuel/cladding interdiffusion.

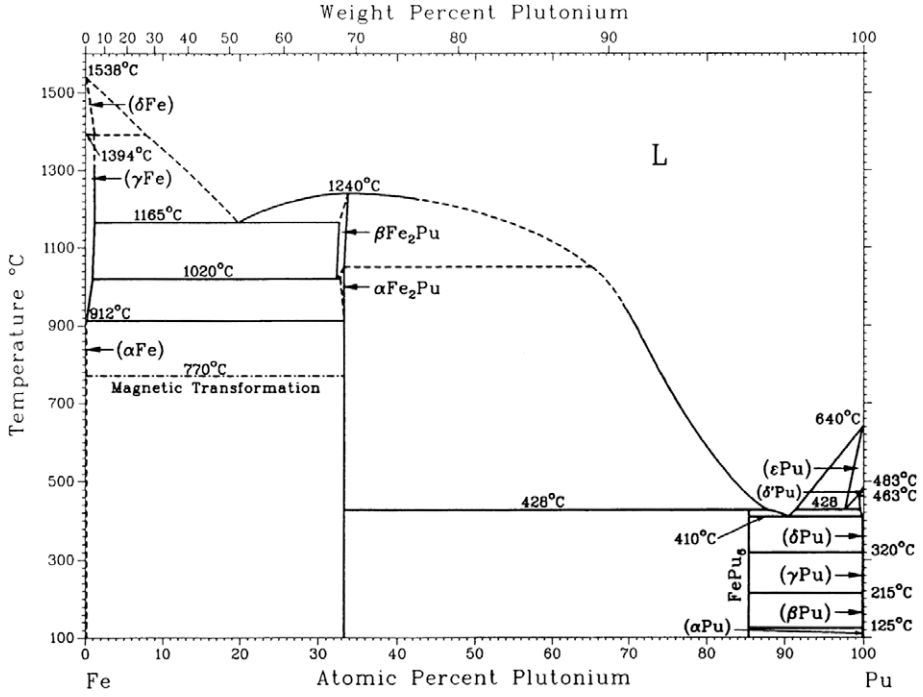

Fig. 9. Fe–Pu phase diagram [47].

4. Conclusions

The experience base for metal alloy fuels provides the basis for utilization of metal fuels at steady state in fast reactors to approximately 10 at.% burnup. Metal fuels have also been demonstrated up to 19 at.% burnup in ferritic–martensitic steel cladding. Minor actinide bearing metal fuel alloys have been tested in limited screening irradiations with no apparent performance issues. Fuel constituent migration, fuel-cladding chemical interaction, and cladding strain are key performance issues to be investigated as MA-bearing metal fuel development is pursued. In addition, fabrication of metal alloy fuel containing americium must be demonstrated at engineering scale. Given these challenges and the historical performance of metal alloy fuel, the prospect for fueling a future fast spectrum reactor using metal alloy fuel is excellent.

Acknowledgments

This submitted manuscript has been authored by a contractor of the US Government for the US Department of Energy, Office of Nuclear Energy, Science, and Technology (NE), under DOE-NE Idaho Operations Office Contract DE-AC07-05ID14517. Accordingly, the US Government retains a nonexclusive, royalty-free license to publish or reproduce the published form of this contribution, or allow others to do so, for US Government purposes.

References

[1] L.C. Walters, B.R. Seidel, J.H. Kittel, Nucl. Technol. 65 (1984) 179.
[2] J.H. Kittel, B.R.T. Frost, J.P. Mustellier, K.Q. Bagley, G.C. Crittenden, J. Van Dievoet, J. Nucl. Mater. 204 (1993) 1.
[3] C.E. Lahm, J.F. Koenig, R.G. Pahl, D.L. Porter, D.C. Crawford, J. Nucl. Mater. 204 (1993) 119.
[4] G.L. Hofman, L.C. Walters, in: R.W. Cahn, P. Haasen, E.J. Kramer (Eds.), Materials Science and Technology, A Comprehensive Treatment, VCH Verlagsgesellschaft mbH, 1994, p. 1.
[5] R.G. Pahl, D.L. Porter, D.C. Crawford, L.C. Walters, J. Nucl. Mater. 188 (1992) 3.
[6] R.G. Pahl, R.S. Wisner, M.C. Billone, G.L. Hofman, in: Proceedings of International Conference on Fast Reactor Safety IV, vol. 129, Snowbird, UT, American Nuclear Society, La Grange Park, IL, 12–16th August 1990.
[7] L.C. Walters, J. Nucl. Mater. 270 (1999) 39.
[8] D.L. Porter, Fuel Test Plan, Argonne National Laboratory, General Electric, and Westinghouse-Hanford Co., June 1994.
[9] A.L. Pitner, R.B. Baker, J. Nucl. Mater. 204 (1993) 124.
[10] D.C. Crawford, D.L. Porter, S.L. Hayes, J. Nucl. Mater. 371 (2007) 202.
[11] H.F. Jelinek, N.J. Carson, A.B. Shuck, Manufacture of EBR-II Core I Fuel, ANL-6274, 1961.
[12] M. Haas, J.D. Cerchione, R.J. Dunworth, R.M. Fryer, C.W. Wilkes, M.H. Derbidge, Fabrication of Driver–Fuel Elements for EBR-II, ANL-79-38, 1979.
[13] R.D. Leggett, L.C. Walters, J. Nucl. Mater. 204 (1993) 23.
[14] R.G. Pahl, D.L. Porter, C.E. Lahm, G.L. Hofman, Metall. Trans. A 21A (1990) 1863.
[15] A.E. Bridges, A.E. Waltar, R.D. Leggett, R.B. Baker, Nucl. Technol. 102 (1993) 353.
[16] R.B. Baker, F.E. Bard, R.D. Leggett, A.L. Pitner, J. Nucl. Mater. 204 (1993) 109.
[17] A.E. Wright, D.S. Dutt, L.J. Harrison, in: Proceedings of International Conference on Fast Reactor Safety IV, vol. 129, Snowbird, UT, American Nuclear Society, La Grange Park, IL, 12–16th August 1990.
[18] T.H. Bauer, A.E. Wright, W.R. Robinson, J.W. Holland, E.A. Rhodes, Nucl. Technol. 92 (1990) 325.
[19] Y.Y. Liu, H. Tsai, M.C. Billone, J.W. Holland, J.M. Kramer, J. Nucl. Mater. 204 (1993) 194.
[20] C.J. Alderman, A.L. Pitner, Trans. Am. Nucl. Soc. 56 (1988) 382.
[21] H. Tsai, L.A. Neimark, T. Asaga, S. Shikakura, J. Nucl. Mater. 204 (1993) 217.
[22] R.V. Strain, J.H. Bottcher, S. Ukai, Y. Arii, J. Nucl. Mater. 204 (1993) 252.
[23] Y.I. Chang, Nucl. Eng. Technol. 39 (3) (2007) 161.
[24] G.L. Hofman, R.G. Pahl, C.E. Lahm, D.L. Porter, Metall. Trans. A 21A (1990) 517.
[25] G.L. Hofman, L.C. Walters, T.H. Bauer, Prog. Nucl. Energ. 31 (1/2) (1997) 83.
[26] Y.S. Kim, G.L. Hofman, S.L. Hayes, Y.H. Sohn, J. Nucl. Mater. 327 (2004) 27.
[27] Y.S. Kim, S.L. Hayes, G.L. Hofman, A.M. Yacout, J. Nucl. Mater. 359 (2006) 17.
[28] R.B. Baker, F.E. Bard, J.L. Ethridge, in: Proceedings of LMR: A Decade of LMR Progress and Promise, Washington, DC, 1990, p. 185.
[29] J.R. Kennedy, J. Cole, A. Maddison, D. Keiser, D. Burkes, Futurix–FTA Metal Alloy Fuel Fabrication and Characterization Report for CEA, INL/EXT-07-12234, February 2007.
[30] C.L. Trybus, J.E. Sanecki, S.P. Henslee, J. Nucl. Mater. 204 (1993) 50.
[31] B.A. Hilton, D.L. Porter, L. Steven, Hayes, Postirradiation Examination of AFCI Metallic Transmutation Fuels at 8 at.%, Presented at the Summer 2006 American Nuclear Conference, Reno, Nevada, June 2006.
[32] B.A. Hilton, D.L. Porter, S.L. Hayes, AFC-1 Transmutation Fuels Post-Irradiation Hot Cell Examination 4–8 at.% Final Report, INL/EXT-05-00785, Rev. 1, September 2006.
[33] H. Ohta, T. Ogata, T. Yokoo, M. Ougier, J.-P. Glatz, B. Fontaine, L. Breton, Nucl. Technol. 165 (2009) 96.
[34] Dominique Warin, CEA, 2006, personal communication.
[35] T. Sofu, J.M. Kramer, J.E. Cahalan, Nucl. Technol. 113 (1996) 268.
[36] K.J. Miles, in: Proceedings of the International Topical Meeting in Safety of Next Generation Fast Reactors, Seattle, WA, American Nuclear Society, La Grange Park, IL, 1–5th May 1988, p. 119.
[37] J.M. Kramer, Y.Y. Liu, M.C. Billone, H.C. Tsai, J. Nucl. Mater. 204 (1993) 203.
[38] S.H. Fistedis (Ed.), The Experimental Breeder Reactor-II Inherent Safety Demonstration, North-Holland, 1987 (reprinted from Nucl. Eng. Des. 101 (1) (1987)).
[39] D.C. Wade, Y.I. Chang, Nucl. Sci. Eng. 100 (1988) 507.
[40] G.H. Golden, H.P. Planchon, J.I. Sackett, R.M. Singer, Nucl. Eng. Des. 101 (3) (1987) 3–12.
[41] M.A. Smith, R.N. Hill, M. Williamson, Low Conversion Ratio Fuel Studies, Argonne National Laboratory Report, ANL-AFCI-163, February 2006.
[42] Y.S. Kim, G.L. Hofman, Thermal Conductivity of TRU–Zr Alloy, Argonne National Laboratory Memorandum, March 14, 2002.
[43] C.M. Walter, G.H. Golden, N.J. Olson, U–Pu–Zr Metal Alloy: A Potential Fuel for LMFBR's, Argonne National Laboratory Report, ANL-76-28, 1975.
[44] W.H. Cubberly et al. (Eds.), Metals Handbook, 9th Ed., vol. 2, ASM International, Materials Park, OH, 1979, p. 783, 833.
[45] J.M. Taylor, A Study of the Kinetic and Mechanical Properties of Stabilized Beta Plutonium Alloy, MS Thesis, University of Idaho, May 1962.
[46] M.C. Billone, W.T. Grayhack, Fuel Creep Model for LIFE–METAL, Argonne National Laboratory Memorandum, March 19, 1987.
[47] M.E. Kassner, D.E. Peterson (Eds.), Phase Diagrams of Binary Actinide Alloys, ASM International, Materials Park, OH, 1995, p. 270, 423, 446.
[48] D.D. Keiser Jr., M.C. Petri, J. Nucl. Mater. 240 (1996) 51.
[49] R.G. Pahl, A Proposed Correlation for U–19Pu–10Zr/D9 FCCI, Argonne National Laboratory Memorandum, 19th March 1990.